

A general regression neural network model offers reliable prediction of CO₂ minimum miscibility pressure

Osamah A. Alomair¹ · Ali A. Garrouch¹

Received: 10 October 2014 / Accepted: 2 August 2015 / Published online: 20 August 2015
© The Author(s) 2015. This article is published with open access at Springerlink.com

Abstract This study introduces a general regression neural network (GRNN) model consisting of a one-pass learning algorithm with a parallel structure for estimating the minimum miscibility pressure (MMP) of crude oil as a function of crude oil composition and temperature. The GRNN model was trained with 91 samples and was successfully validated with a blind testing data set of 22 samples. The MMP for six of these data samples was experimentally measured at the Petroleum Fluid Research Centre at Kuwait University. The remaining data consisted of experimental MMP data collected from the literature. The GRNN model was used to estimate the MMP from the training data set with an average absolute error of 0.2 %. The GRNN model was used to predict the MMP for the blind test data set with an average absolute error of 3.3 %. The precision of the introduced model and models in the literature was evaluated by comparing the predicted MMP values with the measured MMP values and using training and testing data sets. The GRNN model significantly outperformed the prominent models that have been published in the literature and commonly used for estimating MMP. The use of the GRNN model was reliable over a large range of crude oil compositions, impurities, and temperature conditions. The GRNN model provides a cost-effective alternative for estimating the MMP, which is commonly measured using experimental displacement procedures that are costly and time consuming. The results provided in this study support the use of artificial neural networks for predicting the MMP of CO₂.

Keywords General regression neural network · Enhanced oil recovery · Minimum miscibility pressure · Carbon dioxide · Gas injection

Introduction

Enhanced oil recovery (EOR) using carbon dioxide injection can increase the oil production of a reservoir to beyond what it is typically achievable from primary recovery. Compared to other enhanced oil recovery methods, supercritical CO₂ potentially enters zones that have not been previously invaded by water and releases trapped oil. However, a fraction of the injected CO₂ remains stored underground, which is beneficial for the environment. EOR can be achieved using CO₂ injection through two processes, miscible and immiscible displacement, which depend on the reservoir pressure, temperature, and crude oil composition (Andrei et al. 2010). In the 1950s, when CO₂ injection began as an oil recovery method, the immiscible process was emphasized as an alternative recovery scheme for reservoirs where water-based recovery techniques were inefficient (Jarrell et al. 2002). CO₂ flooding is one of the most widely used methods for medium and light oil recovery in sandstone and carbonate reservoirs (Moritis 2006; Alvarado and Manrique 2010). Throughout the last five decades, extensive laboratory studies, numerical simulations and field applications of CO₂ flooding processes have been reported (Burke et al. 1990; Grigg and Schechter 1997; Idem and Ibrahim 2002; Moritis 2006; Chukwudeme and Hamouda 2009; Alvarado and Manrique 2010).

Interest in implementing CO₂ injection as a miscible enhanced oil recovery technique has increased since 1970s (Mungan 1981). CO₂ lowers the interfacial tension (IFT)

✉ Osamah A. Alomair
dr-alomair@hotmail.com; dr.alomair@ku.edu.kw

¹ Petroleum Engineering Department, Kuwait University, Kuwait, Kuwait

and enhances mobility by reducing oil viscosity and causing oil swelling (Simon et al. 1978; Green and Willhite 1998).

Previous research indicated that CO₂ achieves miscibility through multiple contacts with the crude oil in a reservoir (Jarrell et al. 2002). In multi-contact miscibility, the composition of the displacing or displaced fluids is continuously altered. In vaporizing drive by CO₂, miscibility is obtained by vaporizing the light hydrocarbon components into the driving gas. Relative to natural gas and N₂, CO₂ miscibility occurs at a lower pressure. Miscible displacement is characterized by the absence of a phase boundary or interface between the displaced and displacing fluids (Benham et al. 1960). Two fluids are miscible when all mixtures of the two fluids remain in a single phase without any interfaces. In this case, no interfacial tension occurs between the fluids (Stalkup 1983).

Importance of MMP for CO₂ injection

Miscible displacement is only achieved at pressures greater than a certain minimum. The successful design and implementation of a miscible gas injection project depend on the accurate determination of the MMP, which is the lowest possible operating pressure at which the gas can miscibly displace oil.

MMP is also defined as the lowest pressure at which a distinct point of maximum curvature exits in a plot of oil recovery versus pressure. When the maximum curvature point is not obvious, the 95 % oil recovery, which corresponds to 1.2 PV of injected solvent, is used to define the MMP (Lake 1989). A very good oil recovery is guaranteed if the reservoir pressure is greater than the minimum miscibility pressure. MMP is a function of temperature and crude oil properties (Mungan 1981). MMP is an important design factor in the selection of candidate reservoirs for gas injection in which miscible recovery occurs.

MMP is often experimentally estimated using published correlations or modeled using equations of state. Equation-of-state (EOS) calculations are generally conducted by simplifying multicomponent systems into a light component (C₁), intermediate pseudo-component (C₂–C₆), and heavy pseudo-component (C₇₊). An EOS is used to generate the two-phase region (if it exists) for the resulting ternary composition. The critical point and limiting tie line of the mixture are estimated by extrapolating the near-critical data or estimating directly using an EOS (Ahmed 1997). The MMP is generally estimated using this critical region and the solvent/oil compositional data. The EOS technique is plagued by the inaccuracy of gas and liquid data near the plait-point region. These gas and liquid

equilibrium data are often experimental and are time consuming to determine.

Experimental techniques for measuring MMP

Experimental determination of the MMP can be performed using the following typical methods.

- Slim-tube test (Yellig and Metcalfe 1980)
- Micro slim-tube test (Kechut et al. 1999)
- Rising bubble apparatus (Christiansen and Haines 1987)
- Single bubble injection technique (Srivastava and Huang 1998)
- Vanishing interfacial tension methods (Rao 1997)
- Vapor liquid equilibrium-interfacial tension test (Kechut et al. 1999)
- Vapor density of injected gas versus pressure (Harmon and Grigg 1986)
- High-pressure visual sapphire cell (Hagen and Kossak 1986)
- “PVT multi-contact experiments (Thomas et al. 1994)”

The slim-tube method is potentially the primary technique used to determine MMP under reservoir conditions. Slim-tube experiments involve the displacement of live oil from the slim tube by injecting gas at a constant temperature (Thomas et al. 1994). A hybrid slim-tube experimental approach was developed to determine the MMP using a displacement test and the analysis time of the hybrid slim tube was one-tenth shorter than the conventional slim-tube (Kechut et al. 1999). The rising bubble apparatus (RBA) involves injecting a small bubble of gas at the base of a live oil column (Srivastava and Huang 1998). The RBA for MMP was further extended to single bubble injection techniques that estimate MMP by averaging the pressures of bubble disappearance at the bottom and top of the rising bubble column (Srivastava and Huang 1998). To overcome most of the disadvantages in conventional approaches (slim-tube and RBA), a relatively new method, with an elaborative experimental set up but simple technique, was developed by Rao in 1997, called the vanishing interfacial technique (VIT). A prototype of vapor–liquid equilibrium-interfacial tension (VLE-IT) apparatus, proposed by Kechut et al. (1999), is used to measure the interfacial tension (IFT) between the injected gas and oil at a definite temperature, and desired pressures. The plot of IFT values versus pressure is extrapolated to zero IFT. The miscibility of the injected gas and oil is evaluated according to the vanishing IFT between the two phases. The vapor density method is a dynamic test that directly measures the ability of the injected gas to extract intermediate components from the crude oil. The measurements

are conducted in a constant-volume visual PVT cell. In addition to measuring the upper-phase density, the volume of the liquid (lower phase) is monitored to help determine the MMP (Harmon and Grigg 1986). A high-pressure visual cell composed of sapphire was developed to determine the minimum dynamic miscibility pressures (MDMP) by visual observations of gas droplets that pass through the reservoir fluid (Hagen and Kossak 1986). In the Multi-Contact experimental method (Thomas et al. 1994), discrete mixtures of displaced and displacing fluids are combined to determine the MMP.

Correlations used for estimating MMP

Many correlations that relate the MMP to the physical properties of the oil and the displacing gas have been proposed to facilitate screening procedures and to understand the miscible displacement process. The pure CO₂ miscibility pressure was correlated with the temperature, C₅₊ molecular weight, volatile oil fraction, and intermediate oil fraction (Alston et al. 1985). These correlations were also used for impure CO₂ gas streams by including an injection gas critical property function.

The original correlation of Alston et al. (1985) is given by

$$MMP = 6.056 \times 10^{-6} \times (1.8T_R + 32)^{1.06} \times (Mw_{C_{5+}})^{1.78} \times (X_{vol}/X_{int})^{0.136} \tag{1}$$

In the above equation, MMP is in KPa and T_R is in °C. To complete all calculations and analyses in field units, Eq. (1) has been re-arranged and is provided in the “Appendix”.

A correlation (Cronquist 1978) was developed by regression fitting 58 data points. The tested oil gravity varied from 23.7° to 44° API. The reservoir temperature varied from 71 to 248 °F, and the experimental MMP varied from 1073 to 5000 psi. The original correlation (Cronquist 1978) is provided below.

$$MMP = 0.11027 \times (1.8 T_R + 32)^Y \tag{2}$$

In the above notation, MMP is in KPa and T_R is in °C. In Eq. (2), the exponent Y is given by

$$Y = 0.744206 + 0.0011038 \times Mw_{C_{5+}} + 0.0015279 \times vol \tag{3}$$

To complete all calculations and analyses in field units, Eq. (2) has been re-arranged and is provided in the “Appendix”.

A correlation that used temperature as the independent variable and included a bubble point pressure correction was developed and presented in graphical form by Yellig

and Metcalfe (1980). If the oil bubble point pressure exceeded the estimated MMP, the miscibility pressure was set to the bubble point pressure of the oil. Later on, Yellig and Metcalfe (1980) work was given in an equation form by Tarek Ahmed (1997) and is given as follows:

$$MMP = 12.6472 + 0.015531 \times (1.8 T_R + 32) + 1.24192 \times 10^{-4} \times (1.8 T_R + 32)^2 - 716.9427 / (1.8 T_R + 32) \tag{4}$$

In the above equation, MMP is in KPa and T_R is in °C. To complete all calculations and analyses in field units, Eq. (4) has been re-arranged and is provided in the “Appendix”.

Originally, Eq. (5) was used by Newitt et al. (1956) to estimate CO₂ vapor pressure. Later on, in 1984 it was claimed that effects of oil composition on MMP are small at low temperatures (Orr and Jensen 1984). Thus, the vapor pressure at low temperatures may be a good estimate of MMP. It was suggested that the vapor pressure curve of CO₂ can be extrapolated and compared with the minimum miscibility pressure to estimate the MMP for low temperature reservoirs (T < 120 °F). This correlation, referred to as Orr and Jensen (1984) correlation, is given as follows:

$$MMP = 0.10386 \times \exp\left(10.91 - \frac{2015}{255.372 + 0.5556 \times (1.8 T_R + 32)}\right), \tag{5}$$

where MMP is in KPa and T_R is in °C. To complete all calculations and analyses in field units, Eq. (5) has been re-arranged and is provided in the “Appendix”.

A generalized correlation (Glaso 1985) was presented for predicting the MMP required for the multi-contact miscible displacement of reservoir fluids by hydrocarbons, CO₂, or N₂ gas. The original correlation (Glaso 1985) is provided below.

When C₂₋₆ > 18 – mole %

$$MMP = 5.58657 - 0.02347739 \times Mw_{C_{7+}} + (1.1725 \times 10^{-11} Mw_{C_{7+}}^{3.73} \times e^{786.8 \times Mw_{C_{7+}}^{-1.058}}) \times (1.8 T_R + 32) \tag{6}$$

where MMP is in KPa and T_R is in °C. When C₂₋₆ < 18 – mole %

$$MMP = 20.33 - 0.02347739 \times Mw_{C_{7+}} + \left(1.1725 \times 10^{-11} \times Mw_{C_{7+}}^{3.73} \times e^{786.8 \times MW_{C_{7+}}^{-1.058}}\right) \times (1.8 T_R + 32) - 0.836 \times C_{2-6} \tag{7}$$

where MMP is in KPa and T_R is in °C. To complete all calculations and analyses in field units, Eqs. (6) and (7) have been re-arranged and are provided in the “Appendix”.

The above correlations are easy to implement and can be accommodated by simple hand calculations. However, none of these correlations is credible enough to use for the final project design. For screening purposes, these correlations provide a fair guess depending on the data used (Yurkiw and Flock 1994). The success of these correlations is usually limited by the composition and temperature ranges for which they were developed. The objective of this study is to develop a reliable empirical model for predicting the CO₂–oil minimum miscibility pressure using GRNN.

Discussion

Data acquisition

Six fluid samples were collected from various reservoirs in the Middle East. Prior to conducting miscibility studies to determine the MMP of these six fluid samples, detailed and extensive fluid characterization was performed at the General Facility Laboratory in the College of Engineering and Petroleum at Kuwait University. A mercury-free PVT cell was used to determine the thermo-physical properties of the reservoir fluids. Detailed fluid analysis, including the measurement of critical properties, density, viscosity, and molecular weight, was accomplished in our laboratory utilizing a Crude Oil Analyzer that was equipped with a liquid chromatograph for C₃₆₊ measurements and a gas chromatograph for C₁₂₊ measurements.

To determine the MMP data, six multiple contact experiments were performed at various reservoir temperature and pressure conditions. Pure CO₂ was used as the injecting gas. A series of single cell, multiple-contact experiments were conducted. Here, a reservoir fluid sample was loaded into a pressure–volume–temperature (PVT) cell. Next, a sample of pure CO₂ was introduced before allowing the cell to equilibrate at the desired pressure. At this stage, the phase volumes were measured and the equilibrium gas phase was collected in a gas pycnometer before analyzing with a gas chromatograph. Meanwhile, a small liquid sample at equilibrium was collected in a liquid pycnometer and was analyzed using the Liquid Chromatograph. This procedure was repeated again with a new dose of CO₂.

Typically, approximately seven stages or contacts were performed during each experiment. At a certain point, it is observed that both equilibrated phase (liquid and gas) densities converged to the same values, which corresponded to the *K* values as they approached unity. This result implies that both phases become indistinguishable and the boundary between them cannot be ascertained. At

this point, the pressure of the system is recorded and is considered as the MMP.

In addition to the six MMP values measured in our laboratory, MMP data for 107 case studies that were measured using the slim tube, RBA and multi-contact techniques were collected from the published literature (Holm and Josendal 1974; Yellig and Metcalfe 1980; Alston et al. 1985; Glaso 1985; Sebastian et al. 1985; Holm 1987; Zuo et al. 1993; Ahmed 1997; Alomair et al. 2012). The entire data set consisted of 113 samples is given in Table 1. The MMP values were tabulated from these data as a function of crude oil composition, temperature, molecular weights of Mw₅₊ and Mw₇₊, and concentrations of CO₂, H₂S, and N₂.

Data description

This research was based on 113 crude samples for which the MMP values were measured as a function of composition (C₁, C₂, C₃, C₄, C₅, C₆, C₇₊), molecular weight (Mw₅₊, Mw₇₊), temperature, and concentrations of CO₂, H₂S, and N₂. Sample histograms for some of these parameters are shown in Figs. 1, 2, 3, 4, 5, 6. Both MMP and temperature appear to have bimodal distributions (Figs. 1, 2). The molar composition data for C₁, C₂, C₃, C₄, C₅, C₆, and C₇₊ exhibited nearly normal distributions. An example histogram for C₄ is shown in Fig. 3. In addition, the molecular weights for the C₅₊ and C₇₊ pseudo-components appear to be nearly normally distributed (Figs. 4, 5). Generally, the molar concentrations of CO₂, H₂S, and N₂ were positively skewed. An example histogram for CO₂ is shown in Fig. 6. As shown in Table 2, the data set tabulated in Table 1 features few statistical variations in magnitude between the variables. For example, the measured MMP values and the H₂S concentrations vary by three orders of magnitude. Consequently, all variables were standardized to vary within the same order of magnitude (from −1 to +1). The dependent and independent variables were transformed into standardized values using the following equation:

$$\bar{Z} = -1 + 2 \left[\frac{Z - L}{H - L} \right] \quad (8)$$

where \bar{Z} is the standardized variable value, *Z* is the variable value, *L* is the lowest value of a particular variable, and *H* is the highest value of a particular variable

The standardized molar compositions of C₁, C₂, C₃, C₄, C₅, C₆, and C₇₊, the molar concentrations of CO₂, H₂S, and N₂, the molecular weights (Mw₅₊, Mw₇₊), and the temperature were used as input vectors in the GRNN model. The standardized MMP values correspond with the values of the GRNN model output as described below.

Table 1 Data set used for GRNN model development

	Reservoir oil composition												Experimental	
	H2S	CO ₂	N2	C1	C2	C3	C4	C5	C6	C ₇₊	Mw ₅₊	Mw ₇₊	T _R (°F)	MMP (psi)
1	0.001	0.180	0.050	39.58	2.37	1.30	1.30	1.20	1.20	52.80	218	224	170	3015
2	0.001	0.200	0.280	29.45	10.44	12.10	6.70	4.40	3.50	33.00	168	190	130	1723
3	0.001	0.245	0.338	4.07	3.11	4.90	5.70	5.50	5.50	70.70	208	228	160	2100
4	1.370	0.820	0.570	35.13	10.15	7.00	4.30	4.00	3.70	33.10	181	205	188	2147
5	0.001	0.550	0.540	15.94	7.48	5.80	3.20	1.20	6.00	59.40	223	240	106	1215
6	0.001	0.280	0.390	6.29	4.86	4.70	5.90	5.20	3.90	68.50	193	209	160	2300
7	0.001	0.001	0.100	24.15	11.46	8.62	3.77	3.05	3.81	45.04	202	221	104	1799
8	0.001	0.020	0.001	17.04	6.90	6.01	4.31	0.97	5.21	59.54	221	235	109	1300
9	5.730	0.910	1.120	33.34	9.85	6.66	5.20	3.45	3.42	30.32	171	192	245	3400
10	0.001	0.001	0.001	17.07	6.41	7.82	6.72	2.69	5.19	54.10	204	222	109	1500
11	0.001	0.320	0.830	28.65	11.29	12.39	7.82	4.49	4.06	30.15	171	197	130	1600
12	0.001	0.320	0.830	28.65	11.29	12.39	7.82	4.49	4.06	30.15	171	197	130	1800
13	0.001	0.600	3.340	74.16	7.90	4.15	2.15	1.19	0.81	5.70	132	151	155	2234
14	0.001	0.560	3.550	45.34	5.48	3.70	2.35	1.60	0.87	36.12	243	255	140	1978
15	0.001	1.000	0.400	45.40	4.20	0.89	1.08	0.94	1.01	45.08	243	250	196	2768
16	0.001	3.270	0.580	53.89	8.57	6.05	3.49	2.05	1.45	20.66	186	204	221	3629
17	0.001	2.490	0.120	76.43	7.46	3.12	1.80	1.09	0.79	6.70	153	174	265	3286
18	0.001	6.660	0.010	32.98	23.16	8.39	4.23	3.10	1.88	19.59	188	216	180	3190
19	0.001	6.660	0.010	32.98	23.16	8.39	4.23	3.10	1.88	19.59	188	216	240	3705
20	0.001	1.410	0.390	6.35	7.43	7.13	4.62	4.24	2.67	65.76	262	281	240	3675
21	0.300	0.580	0.960	4.49	2.99	4.75	2.73	3.46	14.50	65.24	205	239	138	1697
22	0.120	0.740	2.070	7.49	4.22	7.85	6.55	4.59	10.59	55.78	202	235	145	2060
23	0.160	0.320	0.820	18.59	8.97	8.20	7.13	5.65	7.47	42.69	202	240	153	2393
24	0.001	0.650	0.310	39.14	8.66	6.86	5.10	3.95	4.20	32.02	213	247	182	2842
25	0.001	0.530	1.600	13.22	6.77	6.98	3.91	2.15	5.44	59.40	220	238	89	1499
26	4.500	0.710	0.290	18.29	9.11	5.19	2.78	1.01	7.21	50.93	218	240	92	1512
27	17.560	0.550	0.540	10.78	5.45	7.67	4.56	2.39	3.20	47.35	222	239	88	1493
28	0.001	0.430	1.240	12.98	6.11	9.56	4.19	3.67	4.55	57.27	223	243	93	1509
29	0.001	0.510	0.770	14.73	6.23	7.82	4.49	2.91	1.89	60.77	223	234	77	1378
30	0.001	0.430	0.780	11.98	5.64	9.83	10.10	2.10	3.45	55.69	226	241	92	1515
31	0.230	0.160	0.820	14.22	5.23	8.21	4.39	4.32	4.50	57.90	234	257	77	1398
32	0.050	0.010	14.710	10.11	3.98	5.92	4.10	2.90	3.83	54.38	222	240	71	1198
33	0.001	0.550	0.340	17.11	19.76	7.54	3.76	0.96	6.50	43.48	230	255	91	1567
34	0.001	0.610	0.220	16.01	8.37	5.01	3.12	0.93	7.10	58.70	245	267	88	1642
35	0.010	0.090	0.400	21.00	12.30	4.71	2.90	0.91	4.30	53.40	200	211	96	1547
36	0.001	1.230	0.170	19.34	4.33	6.74	3.11	2.01	4.33	58.74	225	240	80	1420
37	0.001	3.780	0.030	17.13	8.23	3.67	2.81	0.45	7.45	56.45	220	239	112	1855
38	0.070	3.110	0.120	16.01	9.43	4.12	2.81	3.61	2.10	58.62	190	201	99	1399
39	0.090	1.340	0.050	17.39	8.11	4.32	3.10	0.41	7.31	57.88	196	211	83	1195
40	0.001	0.110	10.500	16.24	4.87	3.24	3.13	2.13	7.47	52.41	162	176	116	1598
41	1.040	12.300	2.300	13.89	6.55	4.69	5.69	3.45	8.11	41.98	187	216	103	1411
42	0.001	4.400	0.010	7.90	11.20	6.17	11.23	0.72	15.60	42.77	231	286	99	1649
43	0.090	3.120	2.770	7.55	5.13	3.98	2.76	5.45	6.19	62.96	197	219	176	2300
44	0.001	1.150	1.990	8.10	6.23	4.99	4.34	5.10	7.24	60.86	208	234	167	2298
45	12.300	4.500	0.980	16.44	7.55	3.91	1.70	3.45	2.11	47.06	156	165	169	2160
46	0.001	0.110	4.560	6.00	7.33	4.75	4.79	5.77	7.10	59.59	155	171	178	2205
47	3.310	2.700	4.200	6.98	7.81	4.14	4.10	4.39	8.10	54.27	203	231	183	2491

Table 1 continued

	Reservoir oil composition												Experimental	
	H2S	CO ₂	N2	C1	C2	C3	C4	C5	C6	C ₇₊	Mw ₅₊	Mw ₇₊	T _R (°F)	MMP (psi)
48	0.001	1.210	3.280	6.24	6.16	5.39	3.99	7.18	4.91	61.80	186	207	178	2256
49	0.001	0.910	3.610	12.03	9.92	7.23	4.50	5.81	4.77	51.22	168	186	175	2218
50	5.400	1.100	0.120	29.70	13.23	2.10	1.40	0.76	1.90	44.29	255	265	188	2855
51	0.001	24.000	5.460	4.68	3.78	6.13	7.10	8.22	1.90	38.73	218	256	201	3024
52	5.900	1.070	4.230	4.70	3.78	7.11	8.32	6.82	3.21	54.86	190	211	166	2099
53	0.001	2.360	2.780	8.89	7.07	5.11	4.99	5.78	6.10	56.92	193	217	169	2200
54	0.001	2.910	2.760	12.80	7.12	4.89	4.61	5.20	7.71	52.00	197	226	194	2500
55	0.010	0.070	0.320	16.77	4.40	6.56	6.12	8.13	3.14	54.48	190	213	157	1998
56	1.000	0.190	4.110	5.88	3.39	7.19	6.92	8.17	4.23	58.92	175	196	171	2100
57	9.100	6.670	3.450	2.56	4.11	5.67	6.22	7.10	3.20	51.92	186	208	178	2311
58	0.001	1.520	16.440	5.29	0.01	7.10	6.22	4.51	5.21	53.70	188	208	169	2099
59	0.001	3.310	0.610	11.07	3.23	3.94	0.28	4.11	7.30	66.15	209	231	200	2731
60	0.001	0.670	3.780	5.95	4.46	5.30	5.90	2.13	4.66	67.15	209	222	90	1215
61	0.001	0.910	12.670	5.90	3.71	15.50	6.99	2.18	4.11	48.03	189	203	93	1215
62	12.780	10.020	4.230	4.70	1.77	4.67	8.32	1.51	4.67	47.33	196	211	100	1297
63	0.010	0.070	0.320	9.23	8.12	4.29	4.89	3.67	3.89	65.51	223	240	81	1167
64	1.000	0.190	4.110	5.88	3.39	7.19	6.92	6.90	3.30	61.12	220	244	107	1470
65	0.001	1.190	3.780	6.04	4.46	5.30	5.90	1.16	5.45	66.79	207	219	178	2366
66	0.001	0.245	0.338	4.07	3.11	4.90	5.70	0.93	7.10	73.61	186	197	192	2401
67	0.001	6.000	0.920	31.00	8.68	7.30	4.90	2.01	4.33	34.86	188	207	97	1217
68	2.900	2.780	0.690	29.00	8.15	5.00	3.80	3.61	2.10	41.97	254	278	198	3196
69	1.370	0.820	0.570	25.13	10.15	7.00	4.30	2.90	3.70	44.06	183	199	165	2103
70	0.010	2.390	0.150	23.45	5.37	5.40	3.90	0.41	7.31	51.62	224	245	182	2534
71	0.010	0.550	0.540	15.94	7.48	5.80	3.20	1.16	6.00	59.35	196	209	81	1101
72	2.800	3.170	0.470	29.00	8.75	4.90	3.00	0.25	6.54	41.12	182	198	112	1477
73	0.010	0.310	0.310	16.23	5.95	3.50	7.90	2.13	7.47	56.20	212	234	172	2409
74	1.050	2.780	3.670	22.81	3.93	18.40	3.60	3.45	8.11	32.20	170	201	203	2527
75	0.010	7.230	0.250	32.87	9.38	9.00	5.10	0.72	15.60	19.85	184	265	90	1395
76	0.010	1.860	0.390	34.80	10.39	9.20	5.90	2.69	5.19	54.10	204	222	109	1500
77	0.001	0.060	0.001	0.37	0.37	0.86	2.20	3.42	5.46	87.26	260	278	250	3144
78	0.001	0.480	0.110	16.30	4.03	2.97	3.65	3.73	3.32	65.41	213	227	94	1450
79	0.001	0.840	0.340	49.23	6.32	4.46	7.33	21.47	2.06	31.45	163	230	147	2012
80	0.001	0.001	0.001	52.00	3.81	2.37	7.33	21.47	2.06	36.84	150	199	189	2656
81	0.001	2.440	0.080	82.10	5.78	2.87	1.79	1.12	0.72	4.28	120	138	162	2318
82	0.001	0.270	0.250	25.48	6.96	6.22	4.90	4.33	3.89	55.05	258	285	169	2900
83	0.001	0.001	0.540	0.30	33.66	8.14	4.11	5.08	4.41	37.91	224	260	195	2750
84	2.370	5.780	0.120	27.25	9.51	8.14	5.05	3.85	3.23	34.70	210	237	187	3315
85	0.001	1.460	0.510	17.10	8.01	3.97	2.90	0.93	7.20	57.93	221	240	88	1517
86	0.001	1.970	2.310	14.89	7.31	9.43	4.21	6.90	3.30	49.68	212	240	100	1599
87	0.001	1.310	0.490	21.76	9.13	5.01	1.30	0.25	6.54	54.21	175	186	105	1499
88	0.001	0.910	16.700	5.90	3.71	17.50	6.99	8.16	7.10	32.99	178	224	178	2331
89	0.001	1.010	9.090	4.77	5.61	4.31	6.20	3.10	2.24	63.67	275	291	169	2899
90	5.400	1.100	0.120	29.70	13.23	2.10	1.40	0.59	2.30	44.06	230	240	88	1215
91	0.001	3.100	0.530	27.67	8.16	8.10	5.90	3.60	4.62	42.13	200	223	103	1421
92	0.001	1.190	3.780	6.04	4.46	5.30	5.90	6.20	5.00	62.20	198	220	178	2330
93	0.001	0.690	0.150	45.06	5.37	5.40	3.90	3.00	9.10	27.30	192	241	205	3550
94	0.001	3.200	0.030	27.81	8.21	5.99	4.41	3.60	4.62	42.13	200	223	103	2000

Table 1 continued

	Reservoir oil composition												Experimental	
	H2S	CO ₂	N2	C1	C2	C3	C4	C5	C6	C ₇₊	Mw ₅₊	Mw ₇₊	T _R (°F)	MMP (psi)
95	0.001	1.410	0.390	6.35	7.43	7.13	4.62	4.24	2.67	65.76	262	281	180	3095
96	0.001	0.230	1.590	4.54	2.07	4.41	3.82	9.49	15.30	58.55	189	235	138	1697
97	0.500	0.060	1.560	27.01	11.40	8.96	6.91	4.70	2.77	36.13	206	232	135	2219
98	12.200	1.210	0.420	17.23	8.01	4.47	2.87	1.13	6.98	45.49	218	242	88	1523
99	1.200	13.310	0.010	10.34	6.79	4.57	2.99	1.16	5.45	54.17	223	240	101	1607
100	0.001	0.010	0.740	13.22	6.21	6.71	4.10	2.90	3.70	62.41	195	207	113	1605
101	0.001	0.550	0.540	15.94	7.48	5.78	3.20	1.16	6.00	59.35	223	240	88	1505
102	0.001	1.190	3.780	6.04	4.46	5.30	5.90	6.20	5.00	62.20	198	220	178	2330
103	1.200	3.400	2.000	8.78	9.34	5.11	5.72	5.92	7.40	51.13	211	245	196	2805
104	0.001	7.190	4.820	5.15	7.19	3.80	4.91	5.45	8.00	53.50	199	229	201	2667
105	0.001	1.890	3.230	7.56	6.19	4.50	5.00	5.80	5.33	60.50	170	187	180	2150
106	0.001	2.130	3.670	5.51	3.91	6.10	7.88	4.90	4.90	61.00	183	200	155	2001
107	0.001	24.000	4.360	3.22	3.78	6.13	7.10	4.23	16.00	31.18	181	244	83	1201
108	0.001	2.360	2.780	8.89	2.90	5.11	4.99	3.78	3.38	65.89	186	198	97	1215
109	1.600	2.910	3.560	4.99	6.18	4.89	4.61	2.01	5.27	64.00	222	238	102	1372
110	0.001	1.890	3.230	7.56	6.19	4.50	5.00	0.96	6.50	64.17	189	201	79	1123
111	0.001	0.370	0.980	41.79	8.87	7.10	5.30	0.45	7.45	27.69	207	242	201	2844
112	0.001	0.670	3.780	5.95	4.46	5.30	5.90	6.04	5.70	62.20	196	218	178	2266
113	22.000	0.245	0.338	4.07	3.11	4.90	5.70	0.91	4.30	54.47	159	166	103	1321

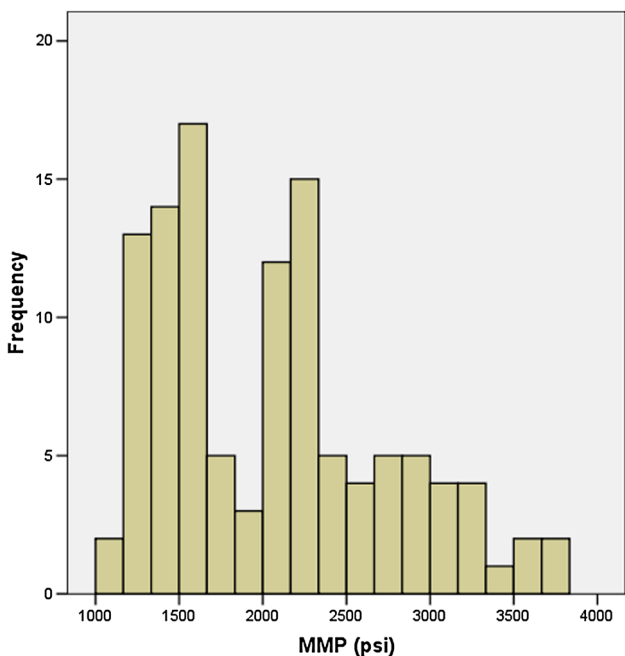


Fig. 1 Frequency histogram of the minimum miscibility pressure (in psi)

GRNN model algorithm

The general regression neural network (GRNN) performs non-linear regressions when the target variables are

continuous. This regression analysis requires that the functional form that mimics the data behavior be estimated. In a multi-dimensional problem, it is difficult to choose this function, which is the main shortcoming of non-linear regression analysis. In contrast, the GRNN algorithm (Specht 1991) successfully overcomes this drawback because it does not require an assumed functional form. The GRNN establishes a functional relationship between the dependent and target variables based on the probability density function of the training data. X in our analysis corresponds to the set of input parameters, described earlier. The random variable Y assumes the value of MMP. An estimate of the pdf (Dai et al. 2010) is given by

$$f(X, Y) = \frac{1}{2\pi^{(\frac{p+1}{2})}\sigma^{(p+1)}} \cdot \frac{1}{n} \sum_{i=1}^n \exp\left(-\frac{D_i^2}{2\sigma^2}\right) \cdot \exp\left[-\frac{(Y - Y^i)^2}{2\sigma^2}\right] \tag{9}$$

where,

σ is the smoothing factor

n is the number of training vectors

p is the dimension of the vector X

Y^i is the output target value for the i th training vector

D_i^2 is the distance between X and the i th training sample X_i , and is given by

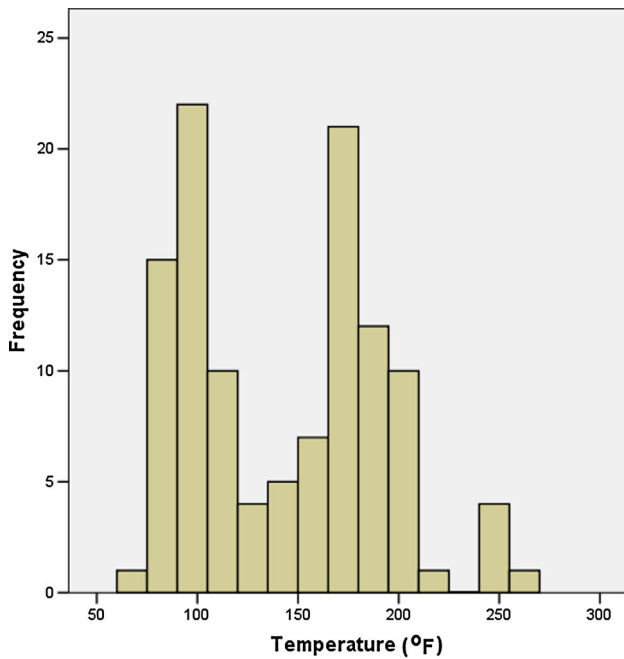


Fig. 2 Frequency histogram for temperature (°F)

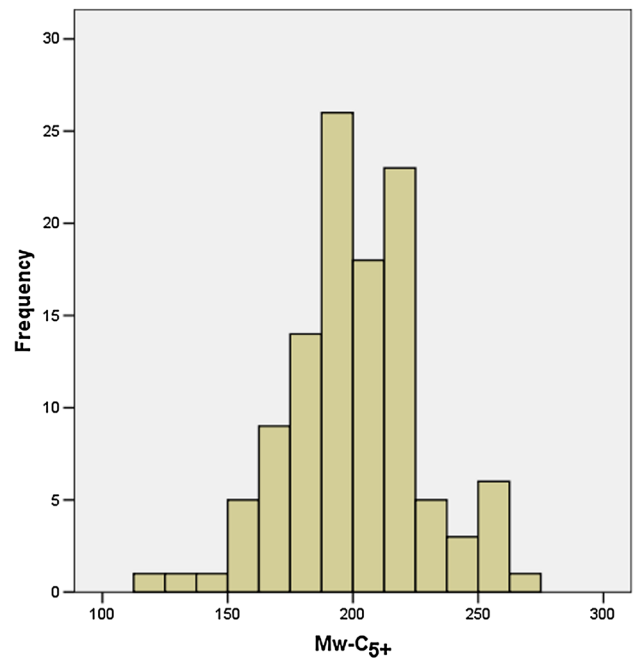


Fig. 4 Frequency histogram for the molecular weights of the C₅₊ pseudo-component

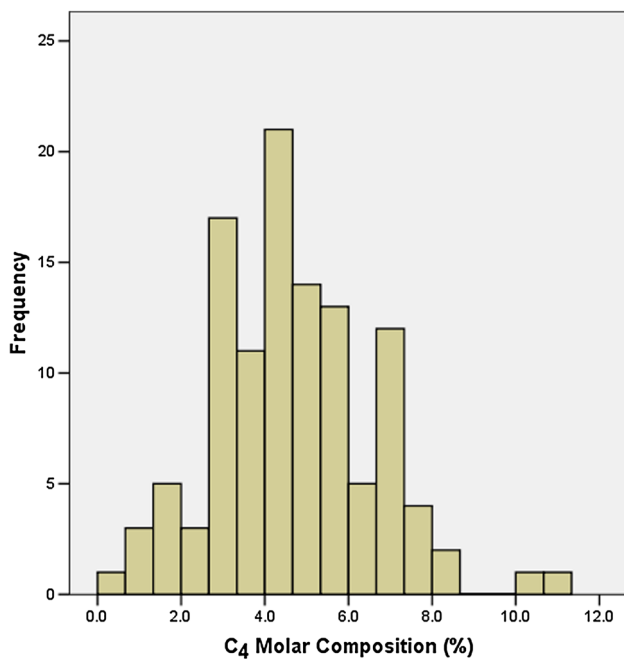


Fig. 3 Frequency histogram for the C₄ molar composition

$$D_i^2 = \sum_{j=1}^p (X_j - X_{ij})^2 \quad (10)$$

Using a nonparametric estimator of the joint probability density function $f(x, y)$, general regressions acquire an estimate \hat{Y} for the conditional mean of a target random

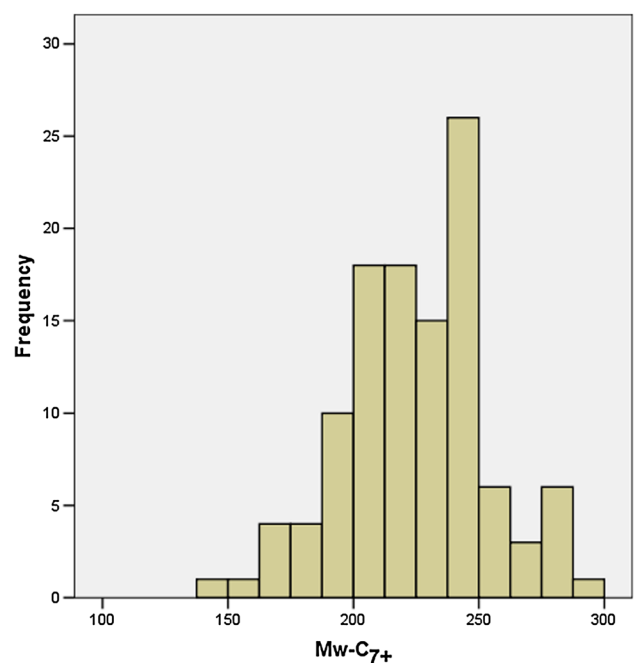


Fig. 5 Frequency histogram for the molecular weights of the C₇₊ pseudo-component

variable Y , when given an input vector of a random variable (X). The class of consistent estimators proposed by Parzen (1962) was used for this purpose. For sample values of X_i and Y_i , the following function was used to estimate the mean of the target random variable ($\hat{Y}(X)$):

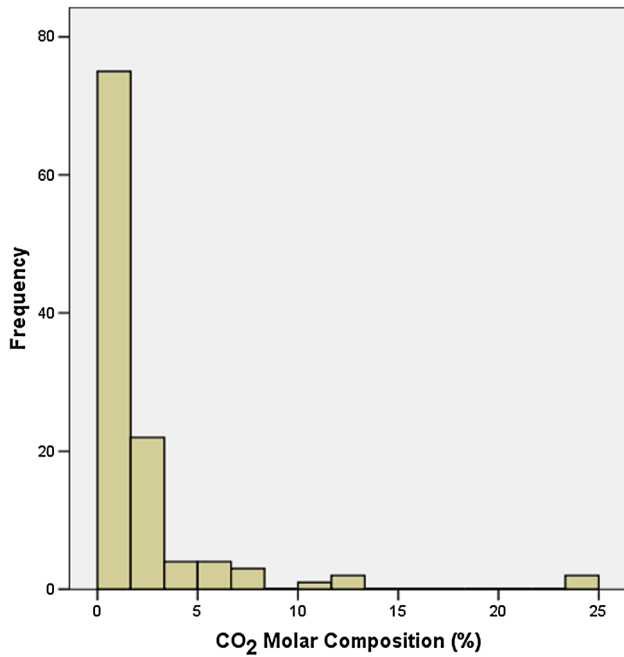


Fig. 6 Frequency histogram for the molar composition of CO₂

$$\hat{Y}(X) = \frac{\sum_{i=1}^n Y_i \exp\left(-\frac{D_i^2}{2\sigma^2}\right)}{\sum_{i=1}^n \exp\left(-\frac{D_i^2}{2\sigma^2}\right)} \quad (11)$$

Equation (11) shows that the general regression is a weighted average of all observed values of Y_i , which are weighted exponentially according to their Euclidean distance from X . For very large standard deviations or a smoothing factor of σ , $\hat{Y}(X)$ converges to the mean of the observed value of Y_i (Specht 1991). In general regression networks, σ is the only important computing parameter that must be optimized (Huang and Williamson 1994). For very large values of n , it is necessary to group observations into a smaller number of clusters to obtain an efficient general regression. The cluster version of a general regression is given as follows:

$$\hat{Y}(X) = \frac{\sum_{i=1}^m A_i \exp\left(-\frac{D_i^2}{2\sigma^2}\right)}{\sum_{i=1}^m B_i \exp\left(-\frac{D_i^2}{2\sigma^2}\right)} \quad (12)$$

In the above equation, parameters A_i and B_i are given by $A_i(k) = A_i(k - 1) + Y_j$ (13)

and

$$B_i(k) = B_i(k - 1) + 1 \quad (14)$$

where

m is the number of clusters

k is the number of observations

A_i and B_i are the sum of the Y values and number of observations grouped into cluster i .

The A_i and B_i coefficients are determined in one pass using the observed samples. A commonly adapted clustering technique consists of arbitrarily setting a single radius, r . When scrolling through the data, the first data point is taken as the first cluster center. If the successive data point has a distance of less than r from this cluster center, the cluster center is updated using Eqs. (13) and (14). Otherwise, the successive data point becomes an additional cluster center (Al-Dousari and Garrouch 2013). The GRNN built based on Eq. (8) through Eq. (12) consists of the following four layers (Fig. 7).

a. An input layer The number of neurons in the input layer is equal to the number of independent variables. Values for these neurons are standardized by subtracting the lowest variable value and dividing by the variable range, as shown in Eq. (8). The input neurons feed these standardized values to each of the neurons in the hidden layer (Fig. 7).

b. A hidden layer This layer associates one neuron for each row in the training data set matrix. The neuron stores the values of the independent variables for a particular row with the corresponding dependent variable values. During training, the GRNN calculates the Euclidean distances for each input neuron of the input vector (X). The distances

Table 2 Statistical summary of the data used to develop the GRNN model

	Mw ₅₊	Mw ₇₊	T _R	MMP	C ₁	C ₂	C ₃	C ₄	C ₅	C ₆	C ₇₊	H ₂ S	CO ₂	N ₂
Mean	201.96	224.67	143.50	2053.35	18.68	7.23	6.12	4.72	3.70	5.18	49.68	1.21	2.20	2.02
Median	199.69	226.00	147.00	2012.00	15.94	6.77	5.40	4.56	3.45	4.66	54.10	0.00	0.91	0.61
Mode	171.20	240.00	178.00	1215.00	4.07	4.46	5.30	5.90	1.16	7.10	62.20	0.00	0.55	0.12
SD	27.38	28.32	47.48	672.98	15.76	4.44	2.82	1.93	3.21	3.03	14.82	3.49	3.79	3.15
Skewness	0.01	-0.19	0.28	0.60	1.74	2.83	1.74	0.40	3.10	1.58	-0.84	3.91	4.00	2.99
Range	154.69	153.03	194.00	2604.00	81.80	33.65	17.54	10.95	21.22	15.28	82.98	22.00	24.00	16.70
Minimum	119.83	137.97	71.00	1101.00	0.30	0.01	0.86	0.28	0.25	0.72	4.28	0.00	0.00	0.00
Maximum	274.52	291.00	265.00	3705.00	82.10	33.66	18.40	11.23	21.47	16.00	87.26	22.00	24.00	16.70

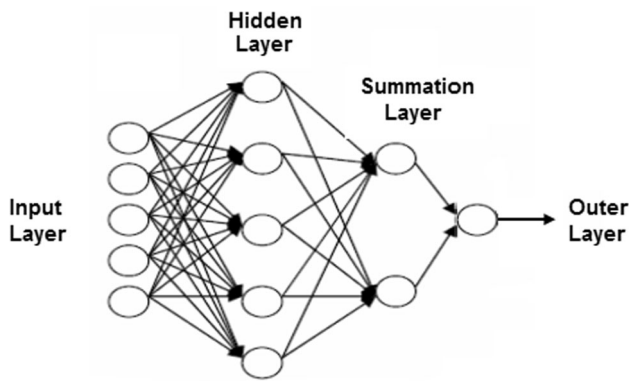


Fig. 7 General regression neural network architecture

from each input neuron are fed with a smoothing factor into a nonlinear exponential activation function, as specified by equation Eq. (12). The resulting value is passed to the neurons in the summation layer (Fig. 7).

c. A summation layer Next, neurons of the summation layer execute the dot product between the weighted A and B coefficients in Eq. (13) and Eq. (14) and the activation results from the input neurons. The summation layer consists of two neurons: a denominator summation unit neuron and a numerator summation unit neuron. The denominator summation unit neuron sums the weight values that arrive from each of the hidden neurons. The numerator summation unit neuron sums the weight values that are multiplied by the actual dependent value for each hidden neuron (Huang and Williamson 1994).

d. An output layer This layer divides the values accumulated in the numerator summation neuron unit by the values accumulated in the denominator summation neuron unit. The resulting values are presented as the predicted output value. The weights of the hidden layer neurons represent cluster centers of a multidimensional space. A and B coefficients related with these clusters are taken as the weights that connect the summation layer and the hidden layer (Huang and Williamson 1994). The smoothing factor is perhaps the most prominent computing parameter for the GRNN's paradigm (Huang and Williamson 1994).

The optimum σ for a GRNN built from a training data set is approximated using an initial guess. Next, the sum squared error (SSE) is calculated for the training data set. This process is repeated by varying σ by a fixed increment. After using a series of trials for σ , the smoothing factor associated with the smallest SSE is used to represent the optimum σ for the training data set. The process of optimizing σ is a default built-in process in NeuroShell toolbox which was used in this study (Ward and Sherald 2006; Al-Dousari and Garrouch 2013).

GRNN model training and validation

An input file, consisting of 113 vectors with 14 attributes, has been downloaded into NeuroShell database (Ward and Sherald 2006; Al-Dousari and Garrouch 2013). NeuroShell randomly splits the data file into a training data set that consists of 80 % of the data (91 vectors), and a blind test data set consisting of the remaining 20 % of the data (22 vectors), used for validation purposes.

Figure 8 compares the estimated MMP using the GRNN model and the MMP values measured experimentally for the training data set. With an average absolute error of approximately 0.2 %, the network appears to mimic the physical relationships between the MMP and the remaining variables. However, this statement is not confirmed unless the model performs well for estimating MMP for the blind test data set. Figure 9 compares the estimated MMP values that resulted from the GRNN model and were measured experimentally for the testing data set. The GRNN model prediction of MMP appears to be very reasonable, yielding an average absolute error of approximately 3.3 %. The GRNN model performance was compared with the MMP

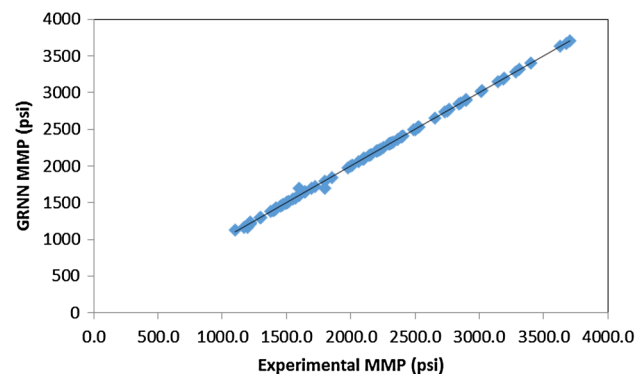


Fig. 8 Comparing the MMP values using the GRNN to MMP data values measured experimentally for the training data set

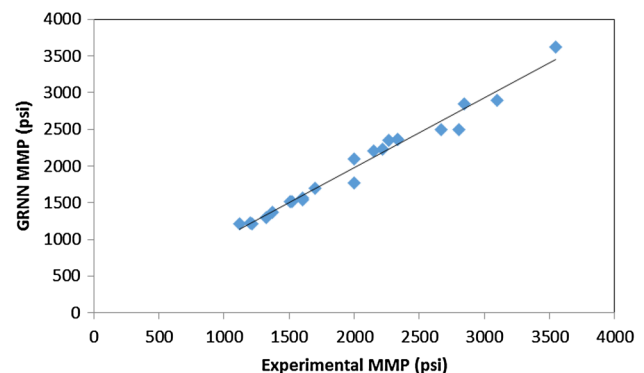


Fig. 9 Comparing the MMP values using the GRNN to MMP data values measured experimentally for the testing data set

correlations (Alston et al. 1985; Cronquist 1978; Orr and Jensen 1984; Glaso 1985). Figures 10, 11, 12, 13, and 14 compare the MMP values predicted by the above models against the experimentally measured MMP values that were determined from the training data set. According to these figures, the predicted MMP values from these correlations are generally unreliable. Table 3 summarizes the average absolute error for these correlations and the GRNN model for the training and testing data sets. The GRNN model prediction is more precise than the other previously mentioned literature correlation methods. The maximum average absolute error when using these correlations varies from approximately 32 to 94 %, which indicates that these predictions are often unreliable. The maximum absolute average error when using the GRNN model on the same data set was approximately 6 %. These results were confirmed by the blind test data set (Table 3). The maximum average absolute error that was obtained using the GRNN model for the testing data set was approximately 12 %.

The reliabilities of each of the literature correlations that were discussed earlier were evaluated using the blind

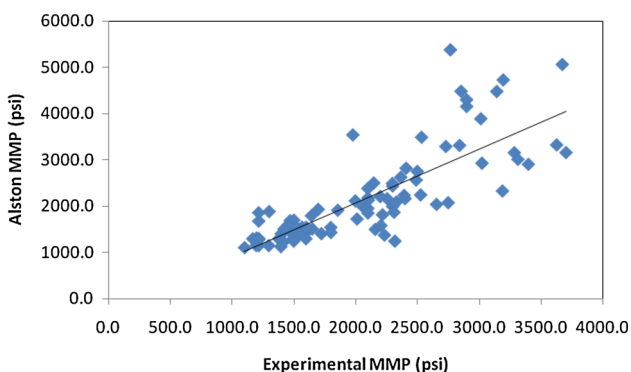


Fig. 10 Comparing the MMP values estimated when using the Alston et al. (1985) model to the MMP data values measured experimentally for the training data set

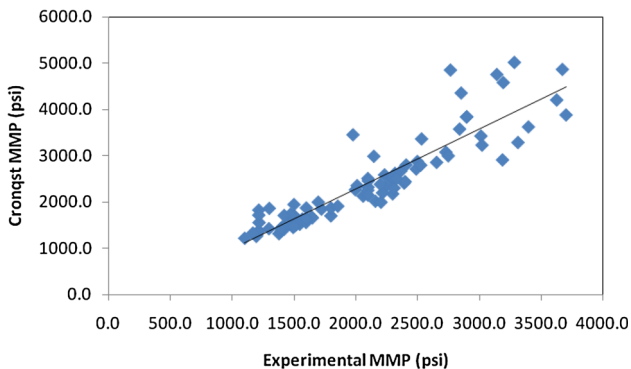


Fig. 11 Comparing the MMP values estimated using the Cronquist (1978) model to the MMP data values measured experimentally for the training data set

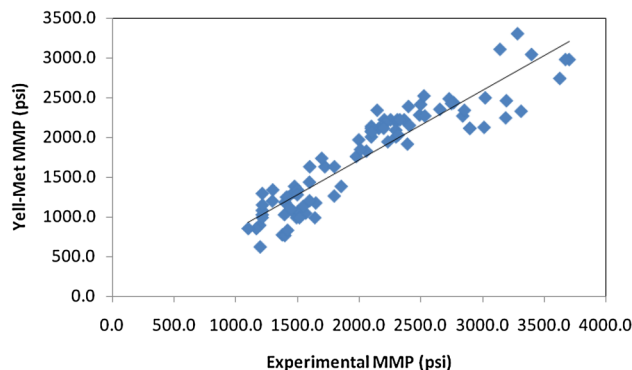


Fig. 12 Comparing the MMP values estimated using the Yellig and Metcalfe (1980) model to the MMP data values measured experimentally for the training data set

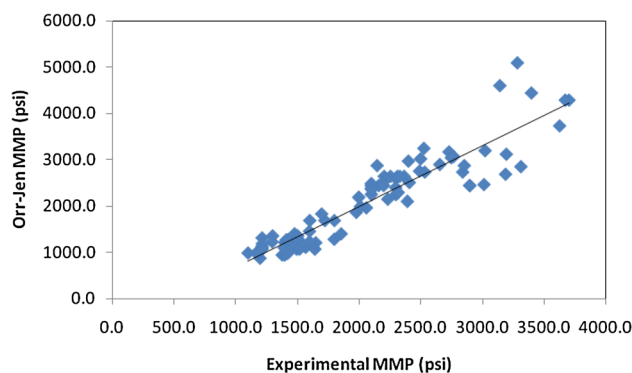


Fig. 13 Comparing the MMP values estimated using the Orr and Jessen (1984) model to the MMP data values measured experimentally for the training data set

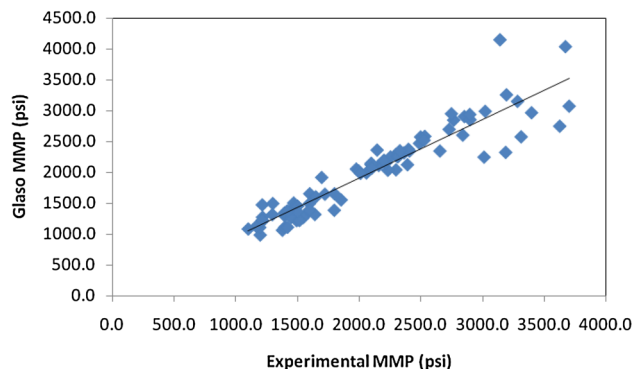


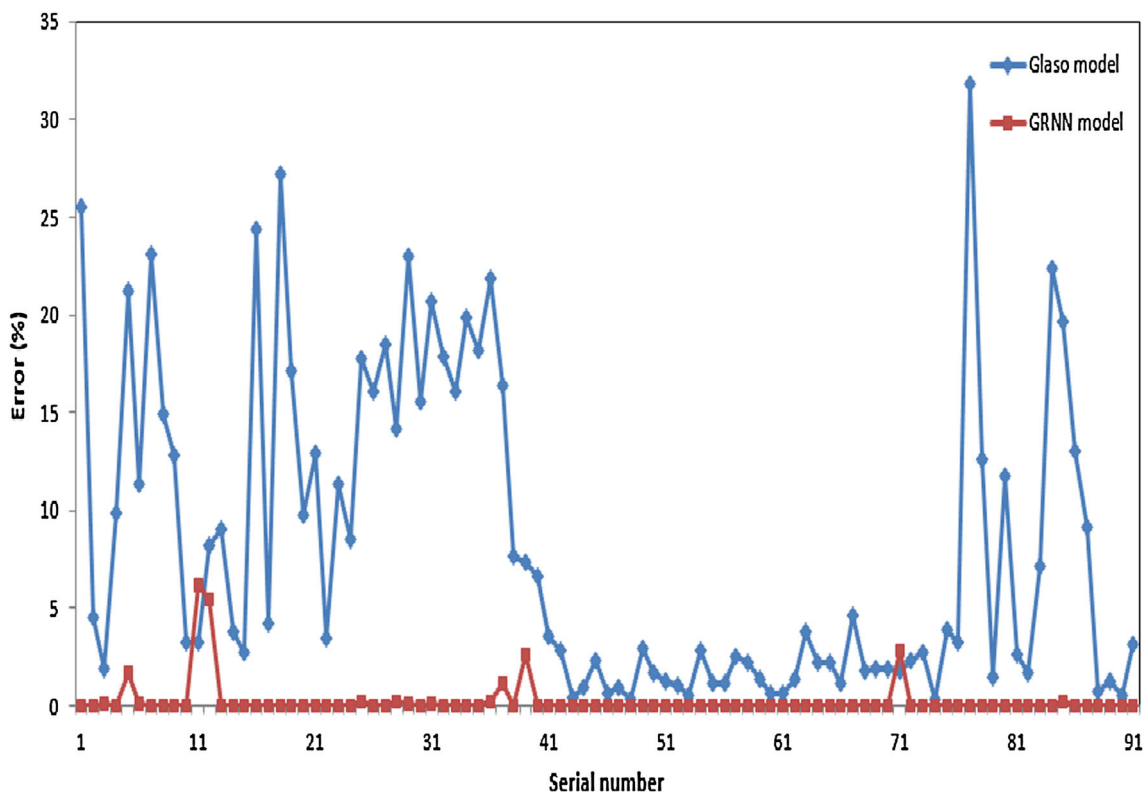
Fig. 14 Comparing the MMP values estimated using the Glaso (1985) model to the MMP data values measured experimentally for the training data set

testing and training data sets. The calculation results are summarized in Table 3 with the minimum error, maximum error, average absolute error, and standard deviation of the error for each correlation. Among the literature correlations that were used, Glaso (1985) correlation yielded the best

Table 3 Average error between the measured data and the predicted data using the GRNN and other models. Results are compared for the training and blind test data sets

	GRNN		Alston		Cronqst		Yell-Met		Orr-Jen		Glaso	
	ϵ	δ_{ϵ}	ϵ	δ_{ϵ}	δ_{ϵ}	ϵ	δ_{ϵ}	ϵ	δ_{ϵ}	ϵ	δ_{ϵ}	ϵ
Training set	0.2	1.0	16.6	17.3	14.4	16.1	15.6	12.2	15.3	10.5	8.1	8.0
Testing set	3.3	3.5	11.5	11.5	9.0	8.4	16.0	12.2	15.4	8.8	7.9	8.5
Max. training	6.2	–	94.2	–	75.3	–	48.2	–	55.0	–	31.9	–
Min. training	0.0	–	0.02	–	0.4	–	0.25	–	0.55	–	0.3	–
Max. testing	12.4	–	43.8	–	38.4	–	37.6	–	36.5	–	32	–
Min. testing	0.3	–	0.4	–	0.2	–	2.0	–	2.2	–	0.39	–

ϵ average error, δ_{ϵ} standard deviation of the average error

**Fig. 15** Comparing the performance of the GRNN model to the Glaso (1985) model for estimating the MMP data using the training data set

results (Table 3). Figures 15 and 16 compare the average absolute errors between the correlation (Glaso 1985) and the GRNN model predictions for the training and testing data sets, respectively. From these figures, the GRNN model outperformed the model (Glaso 1985) by a reasonable margin. However, the correlation (Glaso 1985) presented better prediction accuracy than the other correlations because it accounted for additional effects on the CO₂ MMP that resulted from the presence of intermediate components in the reservoir oil. In contrast, west Texas oils-based correlations (Yellig and Metcalfe 1980)

that included the temperature effects showed the poor performance and may be explained by the dependency of the MMP values on variables that were not included in the correlation. These variables consist of the molecular weight of C₅₊, the oil intermediate fraction, and the paraffinicity. The poor performance model (Orr and Jensen 1984) was likely related to the temperature variations of the data, which vastly exceeded the correlation range of 120 °F. The model (Alston et al. 1985) provided the least adequate predictions, potentially because the correlation was not suitable for flue gas streams that contain N₂.

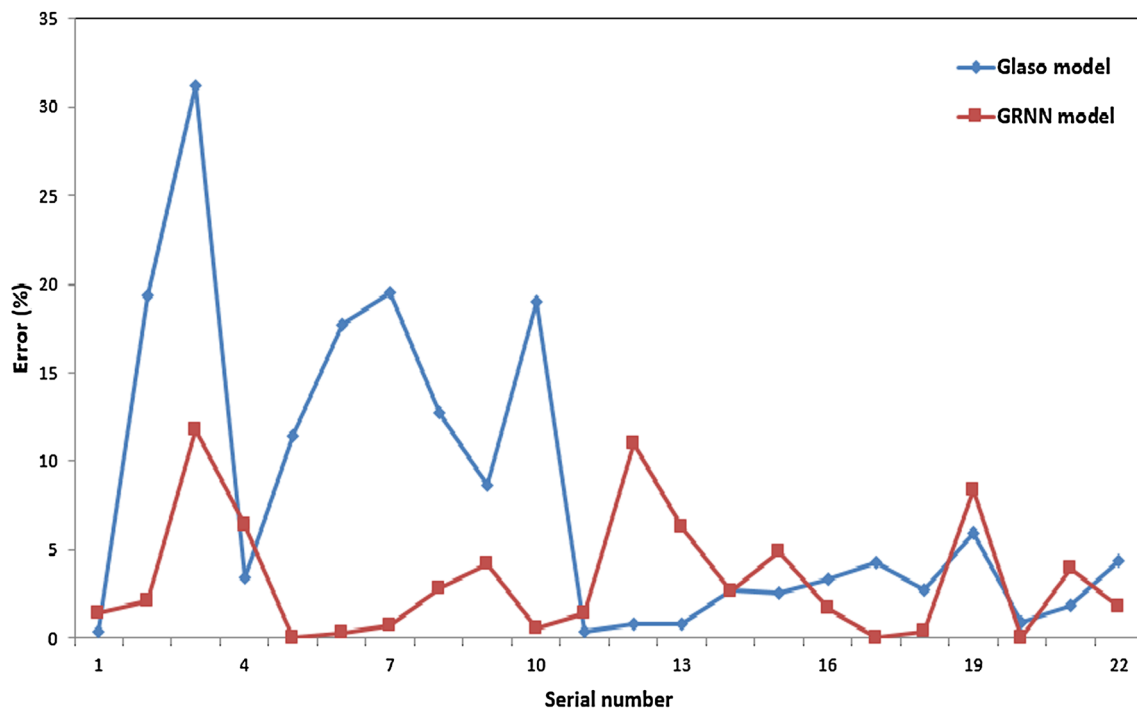


Fig. 16 Comparing the performance of the GRNN model to the Glaso (1985) model for estimating the MMP data using the testing data set

Conclusions

This manuscript introduces a general regression neural network (GRNN) model for estimating the minimum miscibility pressure (MMP) required for the multi-contact miscible displacement of reservoir fluids by CO₂ injection. The model input consists of the reservoir temperature (°F), molecular weight of pentane plus (Mw₅₊), molecular weight of heptane plus (Mw₇₊), mole percent of methane in the crude oil sample, molar percentage of the intermediates (C₂ through C₆) in the oil sample, and the molar percentages of the non-hydrocarbons (CO₂, N₂ and H₂S). The MMP values that are predicted using the GRNN model are compared to experimental data from laboratory tests and MMP data collected from the literature. The GRNN model was able to generalize the training data set results to a new data set that was unseen by the network during training. The GRNN has a parallel structure where the learning is not iterative (i.e., onefold learning going from the input slab to the output slab). This structure allows these networks to learn fast. In addition to fast learning, the

GRNN is efficient for noisy data and performs accurately with light data sets.

Five correlations for predicting MMP that were proposed by a number of investigators were used to predict the MMP for the same data sets that were used by the GRNN model. The GRNN model significantly outperformed all these correlations.

Acknowledgments The authors would like to acknowledge the support of Kuwait University, General Facility Research Grant No. (GE 01/07) through the Petroleum Fluid research Center (PFRC).

Open Access This article is distributed under the terms of the Creative Commons Attribution 4.0 International License (<http://creativecommons.org/licenses/by/4.0/>), which permits unrestricted use, distribution, and reproduction in any medium, provided you give appropriate credit to the original author(s) and the source, provide a link to the Creative Commons license, and indicate if changes were made.

Appendix

See Table 4.

Table 4

Correlation	SI system units (original) Field system units (modifications for this paper)
Alston et al. (1985)	$\text{MMP} = 6.056 \times 10^{-6} \times (1.8 T_R + 32)^{1.06} \times (\text{Mw}_{C_{5+}})^{1.78} \times (X_{\text{vol}}/X_{\text{int}})^{0.136}$ $\text{MMP} = 0.000878 \times (T)^{1.06} \times (\text{Mw}_{C_{5+}})^{1.78} \times (X_{\text{vol}}/X_{\text{int}})^{0.136}$
Cronquist (1978)	$\text{MMP} = 0.11027 \times (1.8 T_R + 32)^Y$ $Y = 0.744206 + 0.00110.38 \times \text{Mw}_{C_{5+}} + 0.0015279 \times X_{C_{1+N_2}}$ $\text{MMP} = 15.988 \times (T)^Y$ $Y = 0.744206 + 0.00110.38 \times \text{Mw}_{C_{5+}} + 0.0015279 \times X_{C_{1+N_2}}$
Yellig-Metcalf (1980)	$\text{MMP} = 12.6472 + 0.015531 \times (1.8 T_R + 32) + 1.24192 \times 10^{-4} \times (1.8 T_R + 32)^2 - 716.9427/(1.8 T_R + 32)$ $\text{MMP} = 1833.7217 + 2.2518055 \times (T) + 0.01800674 \times (T)^2 - 103949.93/(T)$
Orr-Jensen (1984)	$\text{MMP} = 0.10386 \times \exp\left(10.91 - \frac{2015}{255.372 + 0.5556 \times (1.8 T_R + 32)}\right)$ $\text{MMP} = 1071.82893 \times 10^{[2.772 - (1519/(T+460))]}$
Glaso (1985)	$\text{MMP} = 5.58657 - 0.02347739 \times \text{Mw}_{C_{7+}} + \left(1.1725 \times 10^{-11} \times \text{Mw}_{C_{7+}}^{3.73} \times e^{786.8 \times \text{Mw}_{C_{7+}}^{-1.058}}\right) \times (1.8 T_R + 32)$ $\text{MMP} = 20.33 - 0.02347739 \times \text{Mw}_{C_{7+}} + \left(1.1725 \times 10^{-11} \times \text{Mw}_{C_{7+}}^{3.73} \times e^{786.8 \times \text{Mw}_{C_{7+}}^{-1.058}}\right) \times (1.8 T_R + 32) - 0.836 \times C_{2-4}$ $\text{MMP} = 810 - 3.404 \times \text{Mw}_{C_{7+}} + \left(1.7E - 9 \times \text{Mw}_{C_{7+}}^{3.73} \times e^{786.8 \times \text{Mw}_{C_{7+}}^{-1.058}}\right) \times (T)$ $\text{MMP} = 2947.9 - 3.404 \times \text{Mw}_{C_{7+}} + \left(1.7E - 9 \times \text{Mw}_{C_{7+}}^{3.73} \times e^{786.8 \times \text{Mw}_{C_{7+}}^{-1.058}}\right) \times (T) - 121.2 \times X_{C_{2-C_4}}$

References

- Ahmed, T (1997) A generalized methodology for minimum miscibility pressure. Paper No. SPE 39034. In: Fifth Latin American and Caribbean Petroleum Engineering Conference and Exhibition, Rio de Janeiro, Aug 30–Sep 3
- Al-Dousari MM, Garrouch AA (2013) An artificial neural network model for predicting the recovery performance of surfactant polymer floods. *J Pet Sci Eng* 109:51–62
- Alomair O, Malallah A, Elsharkawy A, Iqbal M, Predicting CO₂ minimum miscibility pressure (MMP) using alternating conditional expectation (ACE) algorithm. *Oil Gas Sci Technol* Accepted for publication on December 2012, Published online in June 2013
- Alston RB, Kokolis GP, James CF (1985) CO₂ minimum miscibility pressure: a correlation for impure CO₂ streams and live oil systems. *SPEJ* April issue:268–75
- Alvarado V, Manrique E (2010) Enhanced oil recovery: an update review. *Energies* 3:1529–1575
- Andrei M, De Simoni M, Delbianco A, Cazzani P, Zanibelli L (2010) Enhanced oil recovery with CO₂ capture and sequestration, presented at the World Energy Congress, September 15, p 20
- Benham AL, Dowden WE, Kunzman WJ (1960) Miscible fluid displacement—prediction of miscibility. *Pet Trans AIME* 219:229–237
- Burke NE, Hobbs RE, Kashou SF (1990) Measurement and modeling of asphaltene precipitation. *J Pet Technol* 42:1440–1446
- Christiansen RL, Haines HK (1987) Rapid measurement of minimum miscibility pressure with the rising-bubble apparatus. *SPE Reserv Eng J* 523–527
- Chukwudeme EA, Hamouda AA (2009) Enhanced oil recovery (EOR) by miscible CO₂ and water flooding of asphaltenic and non-asphaltenic oils. *Energies* 2:714–737
- Cronquist C (1978) Carbon dioxide dynamic miscibility with light reservoir oils. In: Proc., Fourth Annual U.S.DOE Symposium, Tulsa
- Dai J, Liu X, Zhang S, Zhang H, Xu Q, Chen W, Zheng X (2010) Continuous neural decoding method based on general regression neural network. *Int J Digit Content Technol Appl* 4(8):1–6
- Glaso O (1985) Generalized minimum miscibility pressure correlation. *SPE J* December issue: 927–934
- Green W, Willhite G (1998) Enhanced oil recovery. *SPE Textbook Series*, 6, Richardson
- Grigg RB, Schechter DS (1997) State of the industry in CO₂ floods. Paper No. SPE 38849. In: SPE Annual Technical Conference and Exhibition, Texas, San Antonio, pp 6–9
- Hagen S, Kossak CA (1986) Determination of minimum miscibility pressure using a high-pressure visual sapphire cell. Paper No. SPE/DOE 14927. In: SPE/DOE Fifth symposium on enhanced oil recovery of the society of petroleum engineers and the department of energy held in Tulsa, OK, pp 20–23
- Harmon RA, Grigg RB (1986) Vapor density measurement for estimating minimum miscibility pressure. Paper No. SPE 15403. In: SPE Annual Technical Conference and Exhibition, New Orleans, pp 5–8
- Holm LW (1987) Miscible displacement. In Bradley HB (ed) *Petroleum engineering handbook*, society of petroleum engineers, Richardson, pp 1–2
- Holm LW, Josendal VA (1974) Mechanisms of oil displacement by carbon dioxide. Paper No. SPE4736. In: SPE-AIME symposium on improved oil recovery, Tulsa, pp 22–24
- Huang Z, Williamson MA (1994) Geological pattern recognition and modelling with a general regression neural network. *Can J Explor Geophys* 30(1):60–68
- Idem RO, Ibrahim HH (2002) Kinetics of CO₂-induced asphaltene precipitation from various Saskatchewan crude oils during CO₂ miscible flooding. *J Pet Sci Eng* 35:233–246
- Jarrell PM, Fox CE, Stein MH, Webb SL (2002) Practical aspects of CO₂ flooding. *SPE Monogr* 22:1–12
- Kechut NI, Zain Z, Ahmad N, Ibrahim DM (1999) New experimental approaches in minimum miscibility pressure (MMP)

- determination. Paper No. SPE 57286. In: SPE Asia Pacific improved oil recovery conference, Kuala Lumpur, pp 25–26
- Lake LW (1989) Enhanced oil recovery. Prentice-Hall Englewood Cliffs, NJ 234
- Moritis G (2006) EOR survey, special report. Oil Gas J 104:37–57
- Mungan N (1981) Carbon dioxide flooding: fundamental. J Can Pet Technol 20(1):87–92
- Newitt DM, Pai MU, Kuloor NR (1956) Thermodynamic Function of Gases. Butterworth's Scientific Publications, London
- Orr FM, Jensen CM (1984) Interpretation of pressure-composition phase diagrams for CO_2 /crude-oil. SPE J October issue: 485–498
- Parzen E (1962) On estimation of a probability density function and mode. Ann Math Stat 33(3):1065–1076
- Rao DN (1997) A new technique of vanishing interfacial tension for miscibility determination. Fluid Phase Equilib 139:311
- Sebastian HM, Wenger RS, Renner TA (1985) Correlation of minimum miscibility pressure for impure CO_2 streams. J Petrol Technol 37(11):2076–2082
- Simon R, Rosman A, Zana E (1978) Phase behavior properties of CO_2 -reservoir oil systems. SPE J 18:20–26
- Specht D (1991) A general regression neural network. IEEE Trans Neural Netw 2(6):568–576
- Srivastava RK, Huang SS (1998) New interpretation technique for determining minimum miscibility pressure by rising bubble apparatus for enriched-gas drives. Paper No. SPE 39566. In: The SPE India oil and gas conference and exhibition, New Dehli, pp 17–19
- Stalkup FI (1983) Miscible displacement, SPE Monograph Series, No. 8, Soc. Pet. Eng., Richardson
- Thomas FB, Zhou XL, Bennion DB, Bennion DW (1994) A comparative study of RBA, P-X, multi-contact and slim tube results. J Can Pet Technol 33(2)
- Ward S, Sherald M (2006) Successful trading using artificial intelligence. Ward Systems Group Inc., Maryland
- Yellig WF, Metcalfe RS (1980) Determination and prediction of the CO_2 minimum miscibility pressures. J Pet Technol January issue:160–168
- Yurkiw FJ, Flock DL (1994) A comparative investigation of minimum miscibility pressure correlations for enhanced oil recovery. J Can Pet Technol 33(8):35–41
- Zuo You-xiang, Chu Ji-zheng, Ke Shui-lin, Guo Tian-min (1993) A study on the minimum miscibility pressure for miscible flooding systems. J Petrol Sci Eng 8(4):315–328